Chinese Chemical Letters 37 (2026) 111927

Contents lists available at ScienceDirect

Chinese Chemical Letters

journal homepage: www.elsevier.com/locate/cclet

# Construction of porous molecularly imprinted polymer on amylose for selective adsorption of estradiol

Xu Guo[a], Dandan Yang[a], Zhongyu He[a], Jie Ding[b], Lan Ding[a,*], Daqian Song[a]

[a] College of Chemistry, Jilin Province Research Center for Engineering and Technology of Spectral Analytical Instruments, Jilin University, Changchun 130012, China

[b] State Key Laboratory of Urban Water Resource and Environment, Harbin Institute of Technology, Harbin 150090, China

ARTICLE INFO

*Article history:*
Received 25 March 2025
Revised 6 July 2025
Accepted 29 September 2025
Available online 29 September 2025

*Keywords:*
Molecularly imprinted polymers
Porous materials
Amylose
Decafluorobiphenyl
17$\beta$-Estradiol

ABSTRACT

The preparation of porous molecularly imprinted polymers (MIPs) from starch, a natural product, presents significant challenges. In this study, we developed a straightforward method for preparing porous MIPs (DFP-MIPs) by crosslinking short amylose as a functional monomer with decafluorobiphenyl (DFP) as a cross-linker. Experimental results indicated that DFP-MIPs exhibited a larger specific surface area (14.06 $m^2/g$) and adsorption capacity (26.3 mg/g), and a high imprinting factor of 3.14 for estradiol (E2), compared to MIPs prepared using tetrafluorobenzenediamine with a single benzene ring as the cross-linker. A method for detecting E2 in milk and meat samples was also established using DFP-MIPs as the adsorbent in conjunction with high-performance liquid chromatography. Under optimal conditions, this method demonstrated a linear range of 0.0200–0.400 μg/g, a detection limit of 0.00300 μg/g, and a recovery rate of 85.2 % to 101.4 %. The proposed method for preparing DFP-MIPs is expected to provide a new pathway for the development of porous and highly selective MIPs using amylose.

© 2026 Published by Elsevier B.V. on behalf of Chinese Chemical Society and Institute of Materia Medica, Chinese Academy of Medical Sciences.

Molecularly imprinted polymers (MIPs) has excellent selectivity because they mimic the interaction between antibodies and biological receptors to recognize the target [1]. Traditional MIPs are prepared by employing self-assembled complexes as precursors, which are formed through hydrogen bonds, hydrophobic or $\pi$-$\pi$ interactions, van der Waals or electrostatic forces between functional monomers and template molecules. Subsequently, these complexes are immobilized by cross-linker [2]. Recently, some researchers have prepared MIPs using estradiol (E2) as a template. The MIPs were prepared by a precipitation polymerisation method using E2 as template, 4-vinylpyridine or methacrylic acid as the functional monomer, ethyleneglycol-dimethacrylate as the cross-linker. The research results indicate that the MIPs can selectively adsorb trace amounts of E2 from samples with complex matrices, such as dairy and meat samples [3]. In order to accelerate the rapid separation of targets from adsorption media, researchers have prepared magnetic MIPs with mesoporous yolk-shell, double yolk-shell and lightweight daisy-like structure for rapid adsorption of E2 in milk powder and environmental water, respectively [4–6]. Although these MIPs have good adsorption performance and selectivity, their preparation uses non-biomass raw materials, which do not meet the requirements of green chemistry and sustainable development, and their large-scale application will be limited [7].

Starch is a renewable biopolymer mainly found in food crops such as potatoes, corn, rice, and wheat [8]. It is a polysaccharide composed of linear amylose and branched amylopectin. Amylose is a linear polysaccharide mainly composed of $\alpha$−1,4-linked-D-glucose units. Amylose can form a single helical structure with many hydrophobic compounds, such as flavor compounds, lipids, and bioactive substances [9–11]. The diameter of the single helix structure is influenced by the size and shape of the encapsulated guest molecules. The single helices can be stacked together to form a V-type crystal structure. Weng *et al.* achieved satisfactory results using the prepared V-type starch as an adsorbent for off-odors of sea cucumber intestinal peptides [12]. However, due to the instability of the helix structure in V-type starch in solution, the adsorbent is not suitable for the adsorption of target compounds in solution environments. Researchers fixed the helical conformation structure through cross-linker and obtained the starch-based MIPs for rebinding of the original encapsulated molecule (template) [13,14]. However, due to the use of flexible crosslinkers such as epichlorohydrin, glutaraldehyde or *N,N'*-methylenebisacrylamide, the MIPs obtained are usually gel phase and lack of porosity, which limits their practical applications.

In this work, a porous bio-based MIPs (DFP-MIPs) was designed and prepared based on helical complexes formed between an-

* Corresponding author.
*E-mail address:* dinglan@jlu.edu.cn (L. Ding).

https://doi.org/10.1016/j.cclet.2025.111927
1001-8417/© 2026 Published by Elsevier B.V. on behalf of Chinese Chemical Society and Institute of Materia Medica, Chinese Academy of Medical Sciences.

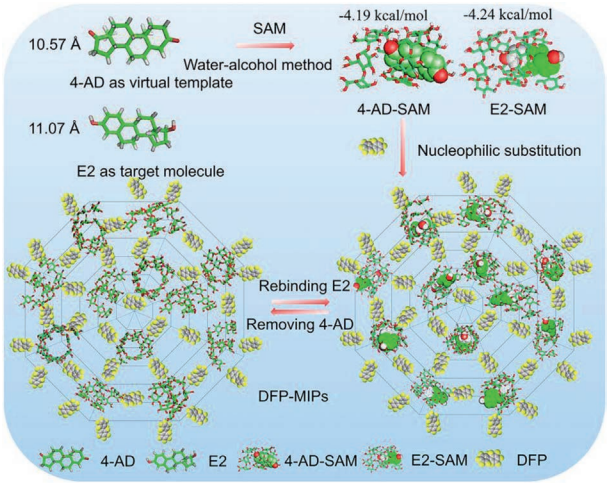



**Fig. 1.** Schematic diagram of DFP-MIPs preparation process.

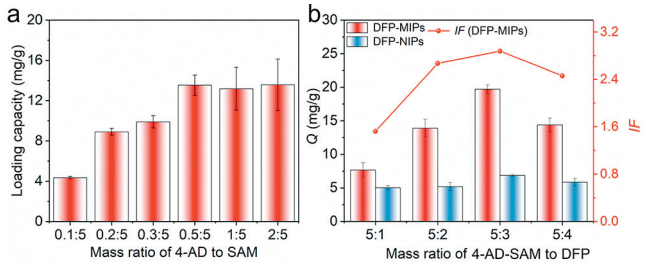



**Fig. 2.** (a) Loading capacity of SAM for 4-AD at different mass ratio of 4-AD to SAM and (b) effect of mass of DFP on the adsorption capacity and imprinting factor of DFP-MIPs at 25 °C.

drostenedione (4-AD) and short amylose (SAM) for selective adsorption of E2. The selection of 4-AD as the virtual template molecule for E2 was driven by three key considerations: Firstly, the binding constant between 4-AD and SAM was determined to be $0.10 \times 10^4$ L/mol, with hydrophobic interaction confirmed (Fig. S1 in Supporting information). Additionally, the sizes of 4-AD (10.57 Å) and E2 (11.07 Å) are very similar (Fig. 1); Secondly, the minimum energy docking conformation of the interaction between SAM and 4-AD or E2 simulated by a molecular docking method shows that the hydrophobic aromatic parts of 4-AD and E2 can enter the hydrophobic helical cavity of SAM to form inclusion complexes; Third, the bonding energies of SAM to form inclusion complexes with 4-AD and E2 are −4.19 and −4.24 kcal/mol, respectively, which are very close (Table S1 in Supporting information). Therefore, 4-AD is suitable as an alternative template molecule for E2, which can avoid the problem of template molecule leakage in the subsequent application of the MIPs.

The preparation of SAM and its inclusion complex with 4-AD (4-AD-SAM) can be found in Supporting information. The preparation of DFP-MIP is as follows [15]: Firstly, Decafluorobiphenyl (DFP) (600 mg), 4-AD-SAM (1.0 g) and $K_2CO_3$ (1.2 g) were added into a flask, and then 30 mL DMF were added under the $N_2$ atmosphere. The mixture was stirred and heated at 85 °C under reflux for 2 days. The obtained suspension was cooled to room temperature and neutralized with 1 mol/L hydrochloric acid until no $CO_2$ bubbles. After centrifugation, the orange product was stirred in water for 15 min, in DMF for 12 h and in dichloromethane for 15 min to remove the hydrochloric and DFP. The product was then soaked in methanol for 24 h until E2 is not detected. The obtained DFP-MIPs was dried at 60 °C for 12 h.

DFP was selected as a cross-linker due to its significant role in the preparation of porous polymer materials [16,17]. DFP is a biphenyl compound containing 10 fluorine atoms. It can undergo nucleophilic aromatic substitution reactions with the hydroxyl groups on the surface of 4-AD-SAM. This process fixes the structure of the 4-AD-SAM helical complex to obtain novel porous DFP-MIPs. The schematic diagram of the preparation process is shown in Fig. 1.

As a comparison, the TFT-MIPs was prepared using 4-AD-SAM as precursor and tetrafluorobenzonitrile (TFT) as a cross-linker. TFT is a compound with a single benzene ring structure containing four fluorine atoms. Its ring length is 12 Å, which is half of DFP (21 Å).

Preliminary experimental results show that the amount of SAM-coated 4-AD is one of the main factors affecting the adsorption capacity and selectivity of DFP-MIPs. Therefore, the maximum loading capacity of 4-AD by SAM was first investigated by fixing the mass of SAM and changing the mass of 4-AD. The loading capacities of 4-AD-SAM were calculated by formula S1 (Supporting information) and the results are shown in Fig. 2a. It can be seen that as the mass ratio of 4-AD to SAM increases from 0.1:5.0 to 0.5:5.0, the loading capacity of SAM on 4-AD gradually increases from 4.4 mg/g to 13.5 mg/g. Further increasing the mass ratio of 4-AD to SAM, the loading capacity of SAM on 4-AD does not increase. Therefore, we chose a mass ratio of 4-AD to SAM of 0.50:5.0 to prepare 4-AD-SAM, which were further used as precursors in the subsequent preparation of DFP-MIPs and TFT-MIPs.

Although the cross-linker do not directly participate in the recognition of target molecules, the adsorption performance of MIPs can be influenced by the strength and density of the imprinted skeleton [18]. Therefore, the mass ratios of 4-AD-SAM to DFP or TFT have also been optimized, respectively. As shown in Fig. 2b and Fig. S2 (Supporting information), as the increase of the mass ratios of 4-AD-SAM to DFP or TFT, the adsorption capacities of DFP-MIPs and TFT-MIPs show a trend of first increasing and then decreasing, reaching its maximum adsorption capacities (19.7 mg/g and 4.0 mg/g) at 5:3, at which point the imprinting factor also reaches their maximum (2.88 and 1.97), respectively. The dosage of DFP or TFT has almost no effect on the adsorption capacity of DFP-NIPs and TFT-NIPs, further proving that the high adsorption capacity and selectivity of DFP-MIPs come from the effective fixation of the helical structure of 4-AD-SAM. Finally, 4-AD-SAM prepared using a mass ratio of 4-AD to SAM at 0.5:5 as the precursor and a mass ratio of 4-AD-SAM to DFP or TFT at 5:3 to prepare DFP-MIPs and TFT-MIPs.

X-ray diffraction (XRD) spectra (Fig. S3a in Supporting information) showed the characteristic diffraction peaks of 4-AD-SAM at $2\theta = 13°$ and 20° are attributed to the V-type crystal structure of amylose, consistent with findings reported in the literature [19]. Circular dichroism results indicate that 4-AD is an achiral compound, SAM exhibits a relatively weak CD signal at 204 nm, but when it forms a helical complex with 4-AD, a strong absorption peak emerges at 291 nm (Fig. S3b in Supporting information), suggesting the formation of a helical structure between 4-AD and SAM.

The morphologies of SAM, 4-AD-SAM, DFP-MIPs and DFP-NIPs were shown in Fig. 3. 4-AD-SAM exhibits an amorphous structure connected together, which is significantly different from SAM with a smooth surface and irregular granular shapes. The phenomenon further proves the formation of a complex between 4-AD and SAM, consistent with the analysis results of XRD (Fig. S3a). Due to the destruction of the V-type structure of 4-AD-SAM after crosslinking by DFP, which was confirmed by XRD (Fig. S4), DFP-MIPs are loose and porous particles with a rough surface, which is significantly different from DFP-NIPs prepared by DFP cross-linked SAM. The same phenomenon also exists in the comparison of scanning electron microscope (SEM) images between TFT-MIPs and TFT-NIPs

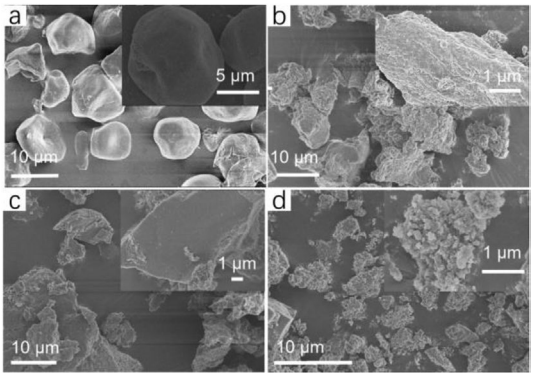



**Fig. 3.** SEM images of (a) SAM, (b) 4-AD-SAM, (c) DFP-NIPs and (d) DFP-MIPs.

(Figs. S5a and b in Supporting information), indicating that the porous structure of DFP-MIPs and TFT-MIPs comes from the fixation of the helical structure formed between 4-AD and SAM by the cross-linker. Compared with TFT-MIPs, DFP-MIPs has a more porous and loose structure, mainly due to the different sizes of cross-linkers used in the preparation process (the length of DFP being twice that of TFT).

To further demonstrate the successful preparation of DFP-MIPs, we tested the water contact angles of SAM, 4-AD-SAM, DFP-MIPs, and DFP-NIPs. As shown in Fig. S6a (Supporting information), the water contact angle of SAM is 83.7° When a helical structure complex is formed between SAM and 4-AD, the hydrophilic hydroxyl groups in SAM are located on the outer surface of the helical structure, leading to an increase in the hydrophilicity of 4-AD-SAM, so the water contact angle of 4-AD-SAM was reduced to 51.3° (Fig. S6b in Supporting information). When 4-AD-SAM was cross-linked with DFP, the hydroxyl position was replaced, resulting in an increase in the hydrophobicity of DFP-MIPs, the water contact angle of DFP-MIPs was increased to 149°, indicating that the MIPs were successfully prepared. This phenomenon also exists in DFP-NIPs.

The Fourier transform infrared spectroscopy (FT-IR) analysis results of DFP-MIPs and DFP-NIPs (Fig. S7a in Supporting information) revealed that the absorption peak at 1488 $cm^{-1}$ and 728 $cm^{-1}$ corresponded to the stretching vibration of the carbon-carbon double bond (C=C) and carbon-fluorine bond group, indicating the successful introduction of DFP into DFP-MIPs and DFP-NIPs. The absorption peak at 3396 $cm^{-1}$ was attributed to –OH stretching vibration, while the absorption peaks at 1150 $cm^{-1}$ and 1021 $cm^{-1}$ were attributed to the C–O stretching vibration. These findings suggest that the skeleton structure of SAM also existed in DFP-MIPs and DFP-NIPs.

Fig. S7b (Supporting information) shows the results of the nitrogen adsorption–desorption experiments of DFP-MIPs and 4-AD-SAM. The Brunauer-Emmet-Teller (BET) surface area, average pore size, and total pore volume of DFP-MIPs (14.06 $m^2/g$, 19.37 nm and 0.068 $cm^3/g$) are greater than those of TFT-MIPs (1.92 $m^2/g$, 14.35 nm and 0.069 $cm^3/g$) and 4-AD-SAM (3.32 $m^2/g$, 17.30 nm and 0.021 $cm^3/g$) (Fig. S8 in Supporting information). However, the nitrogen adsorption-desorption results for the corresponding NIPs were not obtained. The above results indicate that the use of 4-AD-SAM with a helical structure and a larger cross-linker is the key to preparing MIPs with larger BET surface area.

To evaluate the adsorption properties of DFP-MIPs for E2, we first conducted static adsorption experiments. As shown in Fig. 4a, the adsorption capacity of DFP-MIPs, DFP-NIPs, TFT-MIPs, and TFT-NIPs for E2 increases with the initial concentration of E2. DFP-MIPs has a higher adsorption capacity for E2, which indicates that the helical structure formed between SAM and 4-AD and the use of large-sized cross-linkers are the main factors leading to this result.

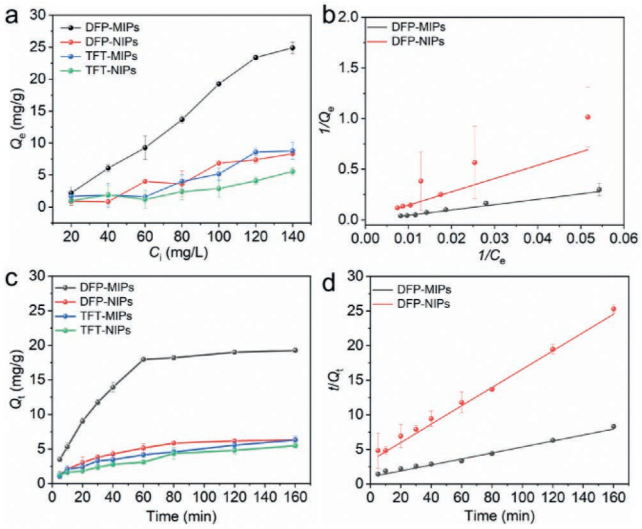



**Fig. 4.** (a) The adsorption isotherms of DFP-MIPs, DFP-NIPs, TFT-MIPs, and TFT-NIPs at 25 °C. (b) Langmuir model of DFP-MIPs and DFP-NIPs. (c) Adsorption kinetics of E2 on DFP-MIPs, DFP-NIPs, TFT-MIPs, and TFT-NIPs at 25 °C (Weight of DFP-MIPs or DFP-NIPs, 5.0 mg; E2 solution, 7.0 mL, 100 mg/L). (d) *Pseudo*-second order model of DFP-MIPs and DFP-NIPs.

Langmuir and Freundlich models were used to fit the static adsorption data of DFP-MIPs. As shown in Fig. 4b and Fig. S9 (Supporting information), the Langmuir model has the highest fitting correlation for the static adsorption data of DFP-MIPs, with a linear correlation coefficient of 0.991. The maximum adsorption capacities of DFP-MIPs and DFP-NIPs for E2 were 26.3 and 8.4 mg/g, respectively, with an imprinting factor of 3.14 (Table S2 in Supporting information).

Dynamic adsorption was used to evaluate the adsorption ability and rate of DFP-MIPs and DFP-NIPs towards E2. As shown in Fig. 4c, within the initial 60 min, the adsorption capacity of DFP-MIPs for E2 increased rapidly and then gradually reached equilibrium. In contrast, DFP-NIPs, TFT-MIPs, and TFT-NIPs not only exhibited significantly lower adsorption capacities than DFP-MIPs but also took up to 80 min to reach adsorption equilibrium. This phenomenon also further indicates that the porosity of DFP-MIPs contributes to the rapid adsorption of E2.

In order to further explore the dynamic adsorption process of DFP-MIPs, *pseudo*-first-order and *pseudo*-second-order-models were used for kinetic fitting. As shown in Fig. 4d and Fig. S9b, the dynamic adsorption process of DFP-MIPs follows the *Pseudo*-second-order model, with a linear correlation coefficient of 0.975, while the fitting correlation of TFT-MIPs is relatively low (Table S3 in Supporting information). The theoretical equilibrium adsorption capacities of DFP-MIPs and DFP-NIPs were calculated to be 21 and 7.6 mg/g, respectively, which are very close to the experimental data.

In order to evaluate the specific recognition ability of DFP-MIPs for E2, selective adsorption experiments were conducted using resorcinol (RF) and dexamethasone (DEX) as structural analogues of E2. From Fig. 5, it can be seen that DFP-MIPs have the highest adsorption capacity for E2, RF and DEX compared with DFP-NIPs. The selectivity factors of DFP-MIPs for RF and DEX are 6.5 and 3.2, respectively.

Variables that affect the adsorption performance of DFP-MIPs were all evaluated with 200 μg/L E2 solution (Fig. S10 in Supporting information). The optimal adsorption conditions of DFP-MIPs for E2 were achieved when the mass of DFP-MIPs was set as 50 mg, the extractive time was 30 min, methanol was used as eluent and 6 min was set as eluent time.

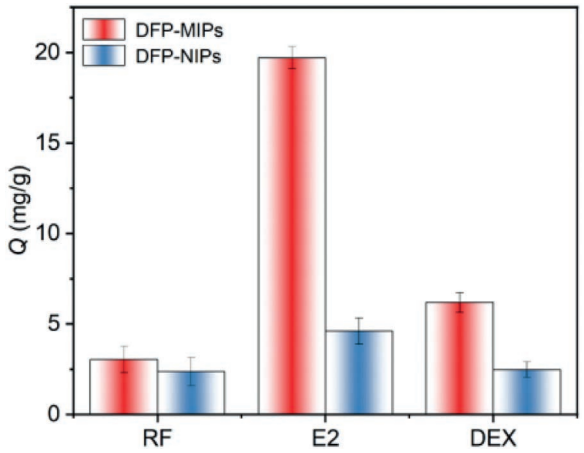



**Fig. 5.** Adsorption capacities of DFP-MIPs for E2 and analogues at 25 °C (Weight of DFP-MIPs or DFP-NIPs, 5.0 mg; E2 solution, 7.0 mL, 100 mg/L).

**Table 1**
Recoveries of E2 in real samples at different spiked levels.

| Sample | Add (μg/g) | Found (μg/g) | Recovery (%) | RSD ($n=3$, %) |
|---|---|---|---|---|
| Pork | 0 | – | – | – |
| | 0.0200 | 0.0186 | 93.0 | 5.8 |
| | 0.200 | 0.201 | 100.5 | 2.8 |
| | 0.400 | 0.406 | 101.5 | 1.3 |
| Beef | 0 | – | – | – |
| | 0.0200 | 0.0170 | 85.0 | 8.2 |
| | 0.200 | 0.197 | 98.5 | 4.5 |
| | 0.400 | 0.402 | 100.5 | 1.6 |
| Milk | 0 | – | – | – |
| | 0.0200 | 0.0186 | 93.0 | 3.3 |
| | 0.200 | 0.200 | 100.0 | 2.7 |
| | 0.400 | 0.400 | 100.0 | 2.3 |

"-" not found.

The reliability of the method was verified by evaluating parameters such as linear range, detection limit (LOD), and quantification limit (LOQ). Under the optimum conditions, E2 showed a good linear relationship in the range of 0.0200–0.400 μg/g, and the correlation coefficient ($R^2$) was above 0.9997. According to the signal-to-noise ratio of 10:1, the LOQ of the method was determined to be 0.0100 μg/g. Based on a signal-to-noise ratio of 3:1, the LOD of the method was determined to be 0.00300 μg/g. The LOQ of this method is lower than the published reports based on MIPs for detecting E2 in complex matrices. The relative standard deviations (RSD) of the intra-day and inter-day for detection of E2 in spiked milk and meat samples (0.200 μg/g) were 3.3 %–3.5 % and 3.7 %–3.8 %, respectively (Table S4 in Supporting information). The recovery and RSD are used to evaluate the accuracy and precision of the method, respectively. The spiked samples at three different concentrations (0.0200, 0.200 and 0.400 μg/g) were analyzed using the proposed method and the results shown in Table 1. The recoveries of E2 in the samples were 85.2 %–101 %, and the RSD was 1.3 %–8.2 %.

Fig. S11 (Supporting information) displayed the chromatograms of the pork samples spiked with 0.200 μg/g E2 before and after adsorption using DFP-MIPs. No peak corresponding to E2 was observed in the extract of the spiked pork sample. However, a distinct E2 peak appeared in the eluent after treatment with DFP-MIPs, and the impurity peaks were significantly reduced, indicating that DFP-MIPs can effectively remove interfering impurities from the pork sample extract. The method was compared with several reported methods for E2 detection in pork and milk samples (Table S5 in Supporting information), demonstrating comparable results in terms of recoveries, RSD, and LODs.

By utilizing the helical complex formed by short amylose and the virtual template 4-AD as a precursor, and cross-linking it with double-benzene ring cross-linker DFP, a porous starch-based DFP-MIPs was successfully prepared. SEM images revealed that the polymer surface was rough with a well-defined porous structure. Further comparison with TFT-MIPs, which were prepared using the single-benzene ring cross-linker TFT, demonstrated that DFP-MIPs exhibited superior adsorption capacity and imprinting factor, indicating that the use of a larger size cross-linker is crucial for achieving excellent adsorption performance and selectivity of DFP-MIPs. DFP-MIPs can be successfully employed as an adsorbent for the rapid separation and enrichment of E2 in milk and meat samples. This preparation method of DPF-MIPs offers a promising and straightforward approach for creating porous MIPs based on short amylose.

## Declaration of completing interest

The authors declare that they have no known competing financial interests or personal relationships that could have appeared to influence the work reported in this paper.

## CRediT authorship contribution statement

**Xu Guo:** Writing – original draft, Methodology, Investigation, Conceptualization. **Dandan Yang:** Writing – review & editing. **Zhongyu He:** Writing – review & editing. **Jie Ding:** Validation. **Lan Ding:** Writing – review & editing, Resources, Data curation. **Daqian Song:** Validation.

## Acknowledgments

The work was supported by the Natural Science Foundation of Jilin Province of China (No. 20220101061JC) and Open Project of State Key Laboratory of Urban Water Resource and Environment, Harbin Institute of Technology (No. HCK202112).

## Supplementary materials

Supplementary material associated with this article can be found, in the online version, at doi:10.1016/j.cclet.2025.111927.

## References

[1] H. Xiong, Y. Wan, Y. Fan, et al., Chin. Chem. Lett. 35 (2024) 108382.
[2] E. Caro, R.M. Marcé, F. Borrull, et al., TrAC Trends Anal. Chem. 25 (2006) 143–154.
[3] Y. Shi, D.D. Peng, C.H. Shi, et al., Food Chem. 126 (2011) 1916–1925.
[4] H.L. de Oliveira, B.C. Pires, C.F. Silva, et al., J. Mol. Struct. 1264 (2022) 133221.
[5] H. Lyu, X. Wu, Y. Yang, et al., New J. Chem. 46 (2022) 11927–11933.
[6] Y. Wang, W. Zhao, R. Gao, et al., J. Hazard. Mater. 424 (2022) 127216.
[7] G. Sennakesavan, M. Mostakhdemin, L.K. Dkhar, et al., Polym. Degrad. Stab. 180 (2020) 109308.
[8] M. Qamruzzaman, F. Ahmed, M.I.H. Mondal, J. Polym. Environ. 30 (2022) 19–50.
[9] L. Shi, H. Hopfer, G.R. Ziegler, et al., Food Hydrocoll. 97 (2019) 105183.
[10] X. Kang, P. Liu, W. Gao, et al., Food Hydrocoll. 99 (2020) 105340.
[11] L. Shi, J. Zhou, J. Guo, et al., Carbohydr. Polym. 274 (2021) 118596.
[12] L. Shi, Z. Li, Z. Yang, et al., Food Chem. 433 (2024) 137171.
[13] Y. Kanekiyo, R. Naganawa, H. Tao, Chem. Commun. (22) (2002) 2698–2699.
[14] Y. Kanekiyo, R. Naganawa, H. Tao, Angew. Chem. Int. Ed. 42 (2003) 3014–3016.
[15] A. Alsbaiee, B.J. Smith, L. Xiao, et al., Nature 529 (2016) 190–194.
[16] D. Shan, S. Deng, J. Li, et al., Carbon 119 (2017) 101–109.
[17] S. Zhou, L. Jin, P. Gu, et al., Chem. Eng. J. 433 (2022) 134442.
[18] N.W. Cheetham, L. Tao, Carbohydr. Polym. 36 (1998) 277–284.
[19] X. Yan, L. Kou, H. Wei, et al., Ind. Crops Prod. 145 (2020) 112097.